Supplementary Information

Hetero-Order Coupled Cavity Electrochromic Mirrors Enabling High-Purity, Wide-Gamut, and Broad-Angle Multicolor Displays

Hangyu Ma,[ab] Shengze Li,[ab] Ying Lv,[*a] Pan Li, [ab] Wentian Zhang, [ab] Guojiao Chen, [ab] Tienan Wang, [a] Xiaoyang Guo, [a] Xingyuan Liu[* a]

[a]*State key laboratory of luminescence science and technology, Changchun Institute of Optics, Fine Mechanics and Physics, Chinese Academy of Sciences, Changchun 130033, China*

[b]*University of Chinese Academy of Sciences, Beijing 100049, China*

**E-mail: lvying@ciomp.ac.cn, liuxy@ciomp.ac.cn*

This file includes:

Methods

Materials. The ITO target with a purity of 99.99% was procured from Changsha Yina Optoelectronic Materials. High-purity WO_3 (99.99%) was supplied by ZhongNuo Advanced Material (Beijing) Technology Co., Ltd., while Sinopharm Group provided the analytical grade solvents, including anhydrous ethanol and diethyl ether. For electrolyte preparation, battery grade, dry lithium perchlorate ($LiClO_4$, 99.99%) and anhydrous propylene carbonate (PC, 99.7%) were acquired from Sigma-Aldrich.

Electrochromic reflector preparation. The electrochromic reflector was deposited onto a K9 glass substrates by electron-beam thermal evaporation method. Unless otherwise specified, the sample dimensions are 17.8 mm × 17.8 mm. Prior to the deposition, the glass substrate underwent a thorough ultrasonic cleaning with acetone, a specialised cleaning solution, a 1:1 volume ratio of ethanol and diethyl ether mixture, and deionised water, followed by drying at 50°C in a vacuum drying oven. Then, the clean glass substrate was secured to a sample holder and placed within the electron beam evaporation chamber. The thin film deposition process commences when the vacuum level falls below 3×10^{-3} Pa. Detailed preparation parameters such as evaporation rates and beam current for each material are listed in Table S1. Film thickness was monitored in real-time using a quartz crystal microbalance positioned at the centre of the chamber. Under identical conditions, patterned electrochromic reflectors were successfully fabricated on a 5 cm × 5 cm substrate *via* mask evaporation.

Characterization. Atomic force microscopy (AFM, SPM790, Shimadzu, Japan), scanning electron microscopy (SEM, S-4800, Hitachi, Japan), X-ray diffractometer (XRD, D8 Focus, Bruker, Germany), X-ray photoelectron spectrometer (XPS, Shimadzu Kratos AXIS SUPRA+), and energy-dispersive X-ray spectrometer (EDX, EMAX, Japan) were

used to characterise the microstructure and elemental composition of the films. The refractive index was measured by spectroscopic ellipsometers (Horiba UVISEL) and fitted with Cauchy model. Electrochemical performance testing was conducted using a standard three-electrode single-cell electrolytic cell. The prepared electrochromic reflective film served as the working electrode, alongside an Ag/AgCl electrode as the reference electrode and a Pt sheet (8 mm × 30 mm) as the counter electrode. The electrolyte was a 1 mol L^{-1} $LiClO_4$ in PC solution. The reflectance spectra of the films at various potentials were measured using an electrochemical workstation (CHI920, Shanghai Chenhua, China), which was coupled with a fiber-optic spectrometer (QE-Pro, Ocean Optics, USA). Relative reflectance was employed for the tests, with a standard aluminum mirror (STAN-SSH) serving as the calibration sample.

Supplementary Notes

Supplementary Note 1. Fresnel equations of multilayer thin film using Transfer Matrix Method (TMM)

$$\mathrm{R} = \left(\frac{\eta_0 B - C}{\eta_0 B + C}\right)\left(\frac{\eta_0 B - C}{\eta_0 B + C}\right)^{*} \quad (1)$$

$$\begin{bmatrix} B \\ C \end{bmatrix} = \left\{\prod_{j=1}^{k} \begin{bmatrix} cos\delta_j & \frac{i}{\eta_j} sin\delta_j \\ i\eta_j sin\delta_j & cos\delta_j \end{bmatrix}\right\} \begin{bmatrix} 1 \\ \eta_{k+1} \end{bmatrix} \quad (2)$$

$$\begin{bmatrix} E_{k-1,k} \\ H_{k-1,k} \end{bmatrix} = \begin{bmatrix} cos\delta_k & \frac{i}{\eta_k} sin\delta_k \\ i\eta_k sin\delta_k & cos\delta_k \end{bmatrix} \begin{bmatrix} E_{k+1} \\ H_{k+1} \end{bmatrix} \quad (3)$$

where $\delta_j = \frac{2\pi}{\lambda} N_j d_j cos\theta_j$, $\eta_j = \begin{cases} \frac{N_j}{cos\theta_j} & (p\_polarization) \\ N_j cos\theta_j & (s\_polarization) \end{cases}$, and *R* is the total reflectance of the film, θ_j (j = 0, 1, 2, 3, 4, 5, 6, 7) is the incident angle of wave propagation in the layer which is determined by Snell's law, d_j is the thickness of each layer, λ is the wavelength of incident light, and $N_j = n_j - ik_j$ (*j*=0, 1, 2, 3, 4, 5, 6, 7) is the complex refractive index of the air, Al_2O_3, Ag, ZrO_2, Ni, ZrO_2, Ni and WO_3 layers, respectively. To simplify this model, the angle of incidence is assumed to be 0° (θ = 0°). Based on the formula: $\eta_j = \begin{cases} \frac{N_j}{cos\theta_j} & (p\_polarization) \\ N_j cos\theta_j & (s\_polarization) \end{cases}$, it can be deduced that $\eta_j\_s = \eta_j\_p$, thereby implying that R = R_s = R_p.

Supplementary Note 2. Comsol Multiphysics electric field simulation

All cross-sectional electric field simulations in this work were conducted with a COMSOL software (4.1a). In the COMSOL 2D multilayer film simulations conducted in this study, periodic boundary conditions were applied to both the left and right sides of the structure. The top and bottom input/output ports were configured for transverse electric polarization, with perfectly matched layers (PMLs) employed to simulate the open air and substrate interfaces.

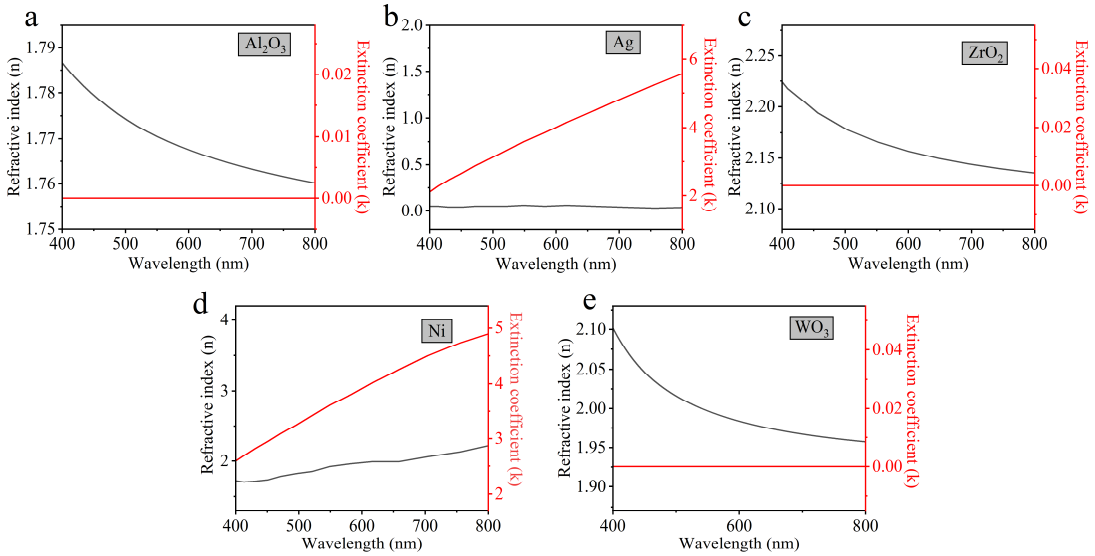

Fig. S1 Complex refractive indices of (a) Al_2O_3, (b) Ag, (c) ZrO_2, (d) Ni, and (e) WO_3.

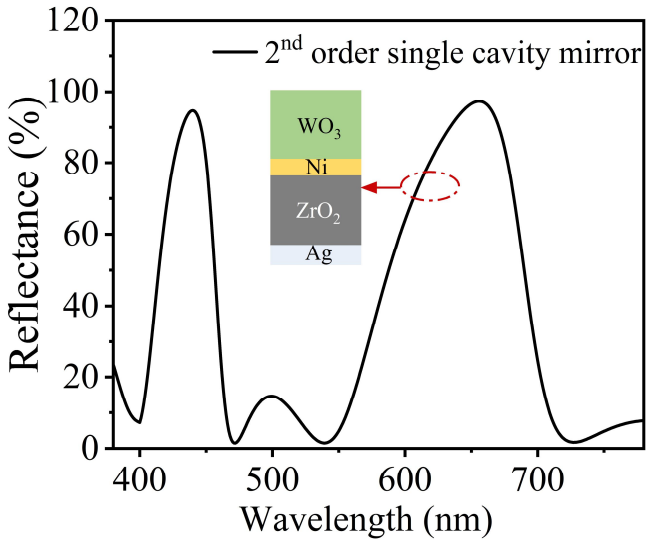

Fig. S2 Simulated reflection spectrum of a 2nd order single cavity mirror.

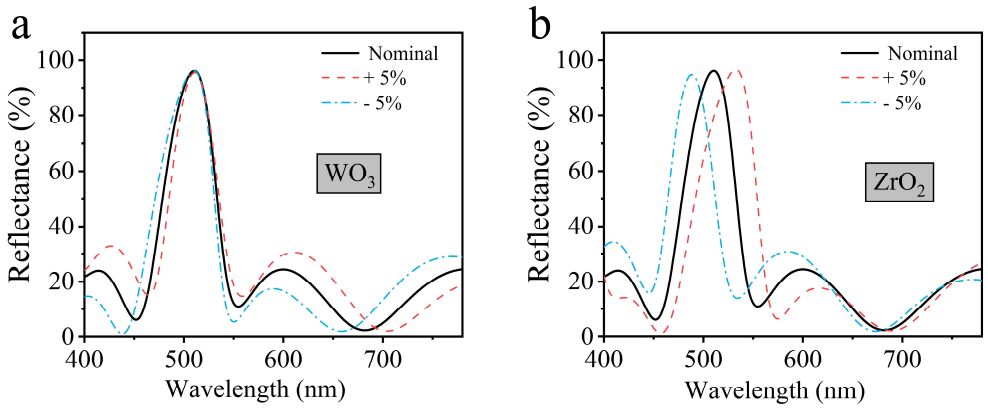

Fig. S3 Reflectance spectra simulated following ±5% variation in (a) WO_3 and (b) ZrO_2 thickness.

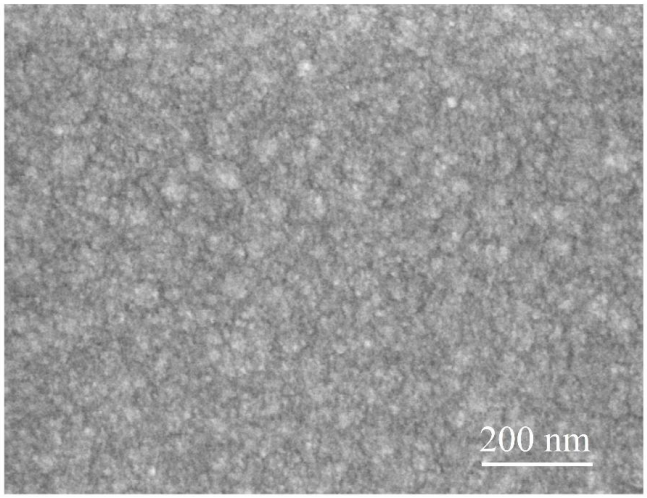

Fig. S4 SEM surface image of HCCECM.

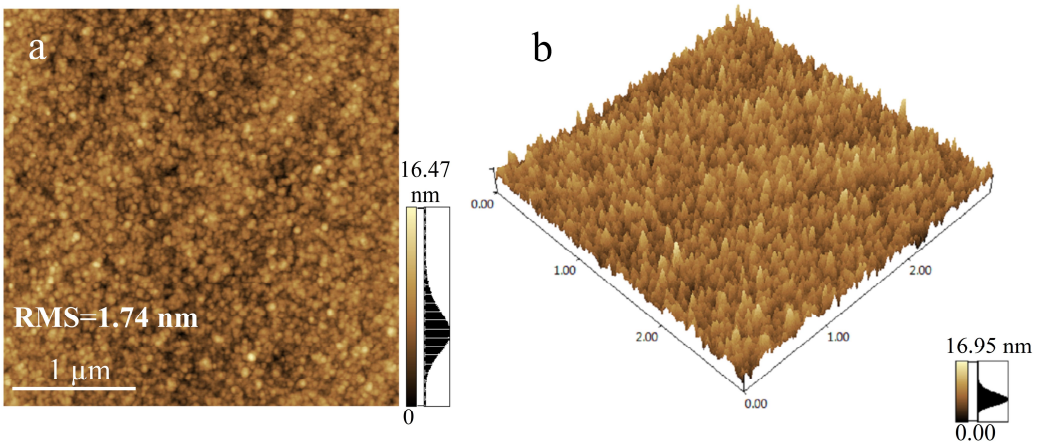

Fig. S5 The surface (a) and 3D (b) AFM images of HCCECM.

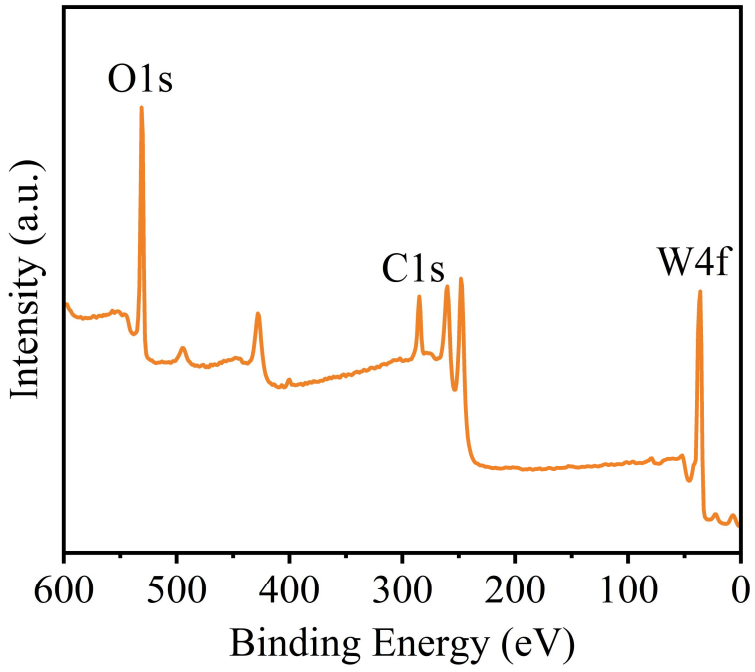

Fig. S6 XPS survey spectrum of HCCECM.

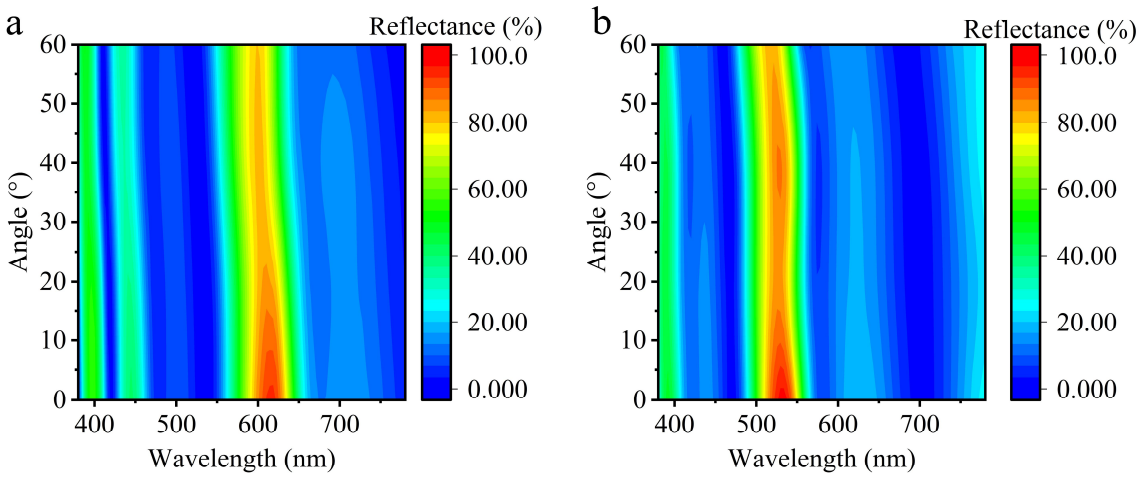

Fig. S7 Angle-dependent reflectance properties of (a) red and (b) green HCCECM.

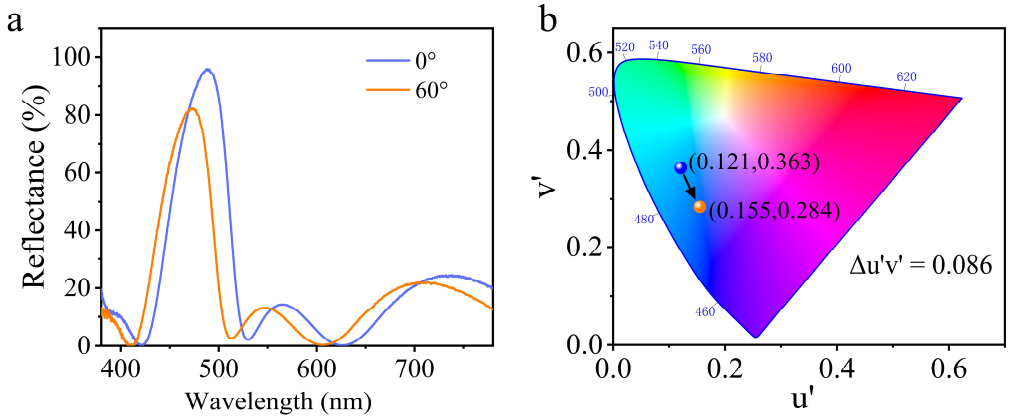

Fig. S8 (a)Reflectance spectra at 0° and 60° viewing angles and (b) their CIE chromaticity coordinates (CIE1976).

To quantitatively evaluate the color stability of HCCECM across different viewing angles, we determined the chromaticity coordinates (*u*', *v*') within the CIE colour space by measuring the spectral reflectance at vertical (0°) and 60° viewing angles according to the CIE 1976 standard. This enabled the calculation of chromaticity deviation (Δ*u*'*v*') to quantify color variation with viewing angle.

$$\Delta u'v' = \sqrt{(u1' - u2')^2 + (v1' - v2')^2} \quad (4)$$

Within the 60° viewing angle range, the maximum chromaticity deviation Δ*u*'*v*' measured for HCCECM was 0.086, which is superior than the viewing angle standard of commercial vertically aligned liquid crystal displays (LCDs, Δu'v'>0.1).

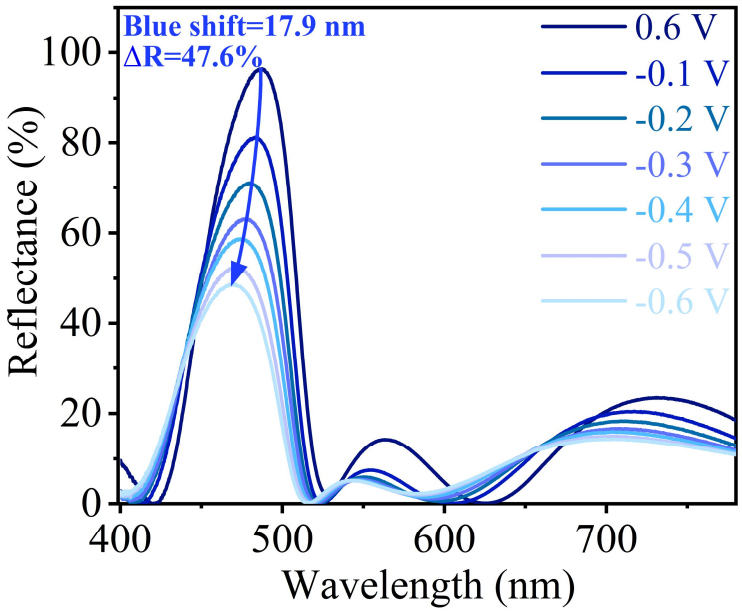

Fig. S9 Reflectance spectra variation of blue HCCECM with potential changes.

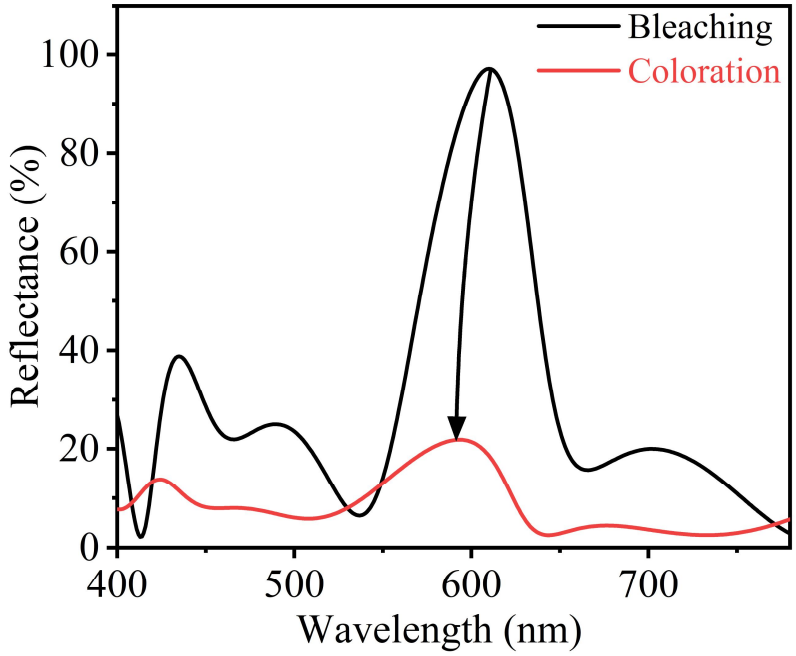

Fig. S10 Simulated reflectance spectra under bleached and colored states.

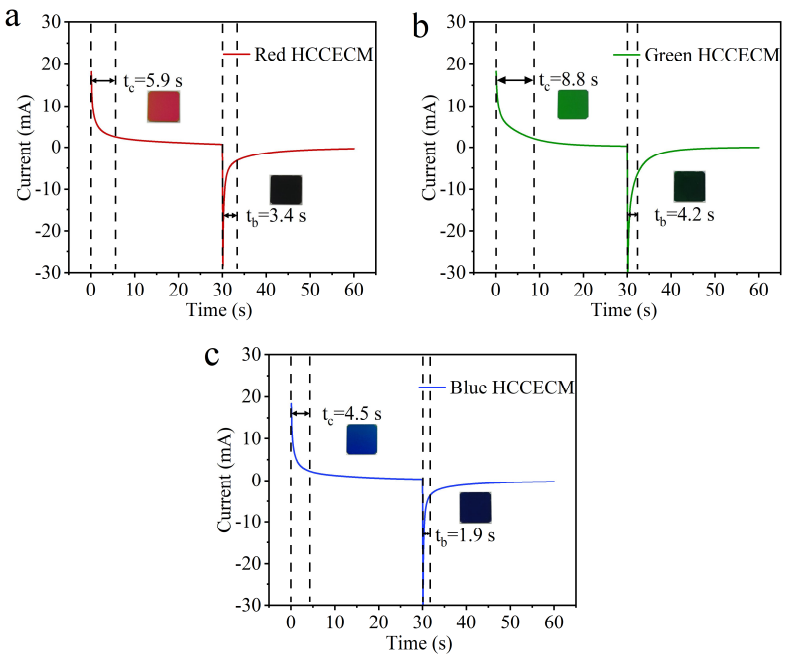

Fig. S11 Current-time curve for (a) red, (b) green and (c) blue HCCECMs under the driving potential of -0.6 and +0.6 V (vs. Ag/AgCl).

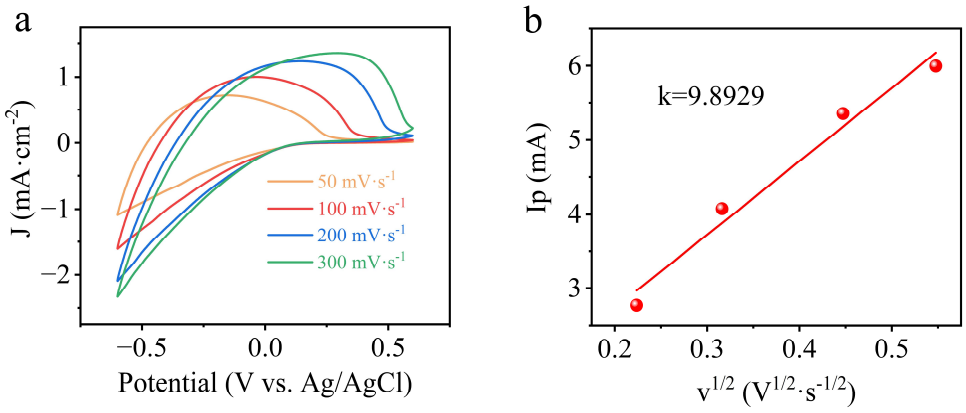

Fig. S12 (a) Cyclic voltammetry (CV) curves of a HCCECM at different scan rates, (b) Relationship between cathode current and the square root of scan rate for of a HCCECM.

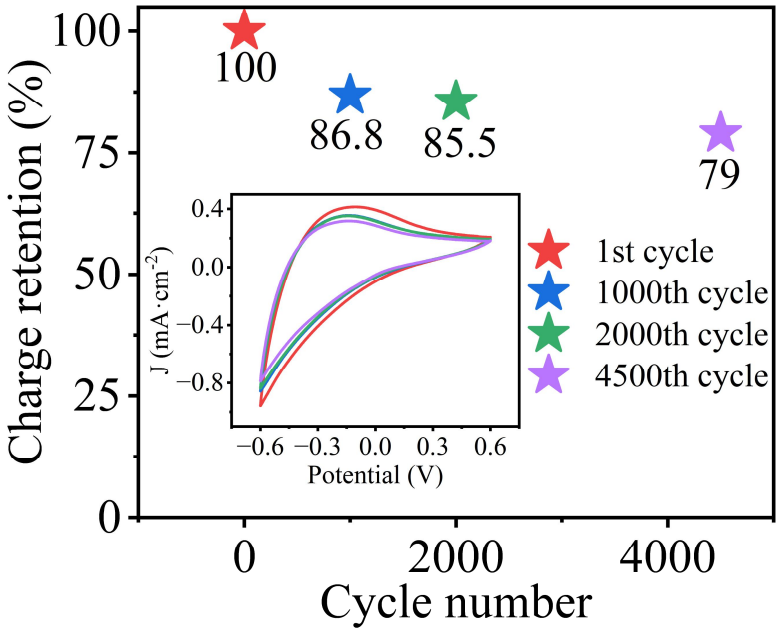

Fig. S13 Charge retention of HCCECM under continuous CV scans. Inserts are relative CV curves.

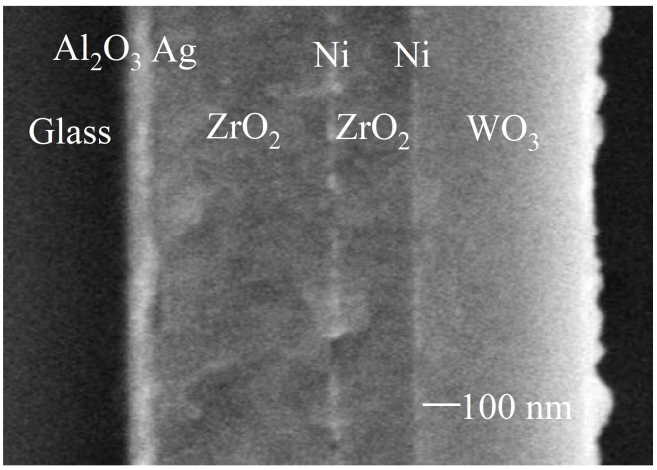

Fig. S14 Cross-sectional SEM image of HCCECM after 5000 cycles under the potential stepping from -0.6 to 0.6 V (vs. Ag/AgCl).

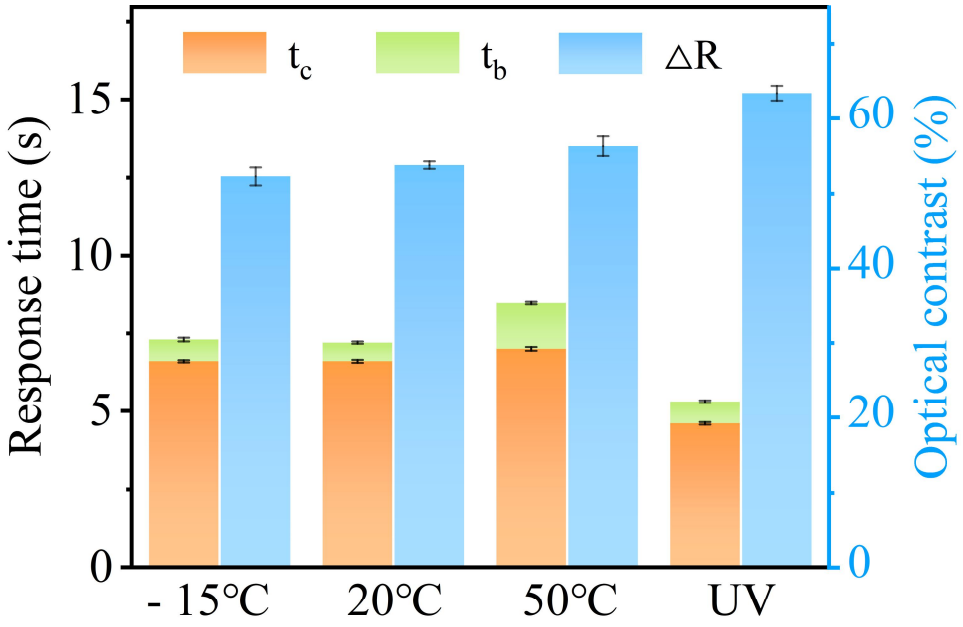

Fig. S15 Coloration/bleaching response time and optical contrast of HCCECM under different temperature and UV exposure (150 W, 355 nm) for 1 hour.

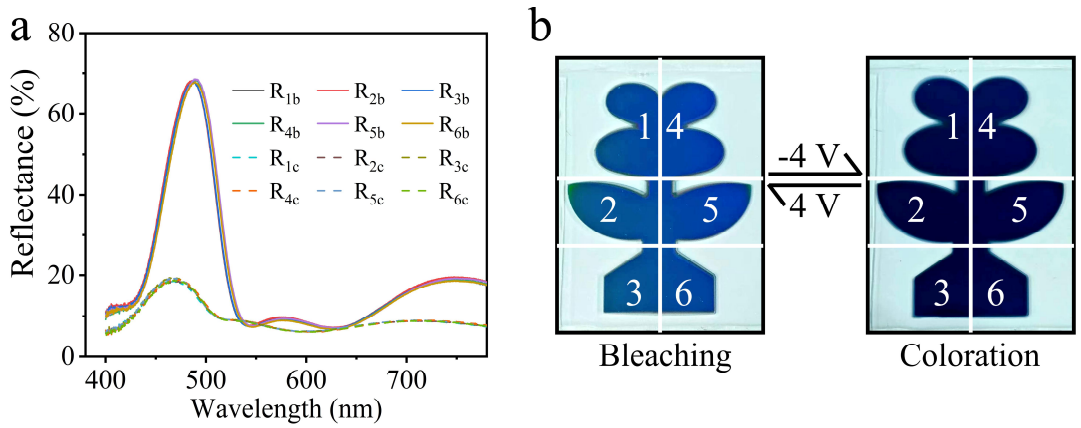

Fig. S16 (a) Reflectance curves and (b) corresponding digital photos in six different regions of the EC device in the bleached and colored state.

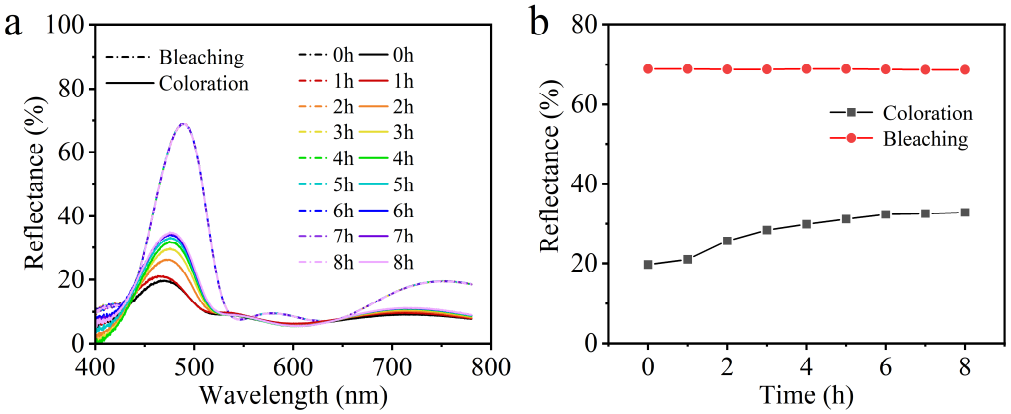

Fig. S17 Optical memory effect of the HCCECM-based EC device. (a) Reflectance spectra measured under open-circuit conditions after bleaching and coloration. (b) Corresponding variation in peak reflectance monitored over 8 hours.

Table S1. Evaporation parameters for materials used in the preparation of HCCECM.

Materials	Evaporation beam current (mA)	Evaporation rate (nm s^{-1})
WO_3	9-10	0.2
Ag	18-20	1.0
Al_2O_3	50-55	0.2
Ni	180-190	0.1
ZrO_2	53-55	0.2

Table S2. Variation in reflector optical performance parameters caused by ±5% changes in WO_3 thickness.

Optical Parameter	Nominal Thickness (nm)	+5% Thinkness (nm)	-5% Thinkness (nm)	Relative Change (from nominal)
Peak Wavelength (nm)	510	511	510	0.2%/0%
Peak Reflectance (%)	95.9	95.3	95.9	-0.6%/0%
FWHM(nm)	56	52	61	-7.1%/8.9%
Q-factor	9.1	9.8	8.4	7.7%/-7.7%

Table S3. Variation in reflector optical performance parameters caused by ±5% changes in ZrO_2 thickness.

Optical Parameter	Nominal Thickness (nm)	+5% Thinkness (nm)	-5% Thinkness (nm)	Relative Change (from nominal)
Peak Wavelength (nm)	510	533	488	4.5%/-4.3%
Peak Reflectance (%)	95.9	96.3	94.6	0.4%/-1.4%
FWHM(nm)	56	64	50	14.3%/-10.7%
Q-factor	9.1	8.3	9.8	-8.8%/7.7%

Table S4. Summary of simulated reflective performances of HCCECMs with different reflective peak wavelengths.

Peak wavelength (nm)	peak reflectance (%)	FWHM (nm)	Q -factor
461	95.0	56	8.2
496	94.9	62	8.0
507	95.6	62	8.2
529	96.6	64	8.3
572	95.0	71	8.1
595	95.0	74	8.0
644	94.9	78	8.3